Supplementary Information (SI) for EES Catalysis.

Supporting Information

Atom-Economical Insertion of Hydrogen and Sulfur into Carbon-Nitrogen Triple Bonds Using H_2S via Synergistic C-N Sites

Ganchang Lei[a], Jiayin Wang[a], Xinhui Liu[b], Shiping Wang[a], Shijing Liang[a], Lijuan Shen[b], Yingying Zhan*[a], Lilong Jiang*[a]*

[a]National Engineering Research Center of Chemical Fertilizer Catalyst, School of Chemical Engineering, Fuzhou University, Gongye Road 523, Gulou District, Fuzhou, Fujian 350002, P. R. China.

[b]College of Environmental and Resource Science, College of Carbon Neutral Modern Industry, Fujian Key Laboratory of Pollution Control & Resource Reuse, Fujian Normal University, 350007, Fuzhou, Fujian, People's Republic of China.

L. Shen. E-mail: syhgslj@fzu.edu.cn

Y. Zhan. E-Mail: zhanyingying@fzu.edu.cn

L. Jiang. E-mail: jll@fzu.edu.cn

Experimental section

Chemicals and reagents

Dicyandiamide (≥ 98.0%) and glucose (≥ 99.0%) were purchased from Sinopharm Chemical Reagent (Shanghai, China). Ethanol (> 99.5%), N,N-Dimethylformamide (DMF, ≥ 99.9%), Dimethyl sulfoxide (DMSO, > 99.8%) and Dimethylacetamide (DMAC, ≥ 99.9%) were collected from Sinopharm Chemical Reagents, China. Isopropylamine (C_3H_9N, ≥ 99.0%), Benzonitrile (C_7H_5N, ≥ 99.0%), 4-methoxybenzonitrile (C_8H_7NO, ≥ 99.0%), 4-chlorobenzonitrile (C_7H_4ClN, ≥ 98.0%), 4-hydroxybenzonitrile (C_7H_5NO, ≥ 98.0%), 4-ethylbenzonitrile (C_9H_9N, ≥ 98.0%), 4-bromobenzonitrile (C_7H_4BrN, ≥ 97.0%), 4-flurobenzonitrile (C_7H_4FN, 99.0%), 2-flurobenzonitrile (C_7H_4FN, ≥ 99.0%), 4-phenoxybenzonitrile ($C_{13}H_9NO$, ≥ 98.0%), 4-amino-2-chlorobenzonitrile ($C_7H_5ClN_2$, 99.0%), acetonitrile (C_2H_3N, 99.8%), 2-methylpropanenitrile ($(CH_3)_2CHCN$, 99.6%) and ethyl cyanoformate ($C_3H_5NO_2$, 98%) were collected from Aladdin (Shanghai) Chemistry Co., Ltd. Deionized water was provided from local sources. N_2 gas (≥99.9%) was purchased from Linde Industrial Gases (Xiamen, China). A reaction gas containing H_2S (50000 ppm) and N_2 (balance) was supplied from Dalian Special Gases (Dalian, China). All chemicals were used as received without further treatment.

Synthesis of samples

N-GC-$_X$ were prepared by carbonizing the mixture of dicyandiamide and glucose. Typically, 1 g of glucose with designed amounts of dicyandiamide (i.e., 0, 2, 4, 6, and 8 g) were mixed well, and then the mixture was transferred into the tube furnace under flowing N_2. The temperature of the tube furnace experienced the following heating procedures: from room temperature to 600 °C (2.3 °C/min), from 600 °C to 780 °C (2 °C/min), and kept at 780 °C for 60 min. The collected N-GC-$_X$ are herein denoted as pristine GC, N-GC-2, N-GC-4, N-GC-6, and N-GC-8 for dicyandiamide = 0, 2, 4, 6, and 8 g, respectively.

Characterization

The total pore volume and BET surface area were evaluated on a Micromeritics ASAP 2020 system at 77 K. The Scanning electron microscope (SEM) was performed on JSM-6700. Transmission electron microscope (TEM) was carried out over a JEM 2010EX. The X-ray diffraction (XRD) patterns were obtained on a X'PertPro diffractometer using Cu Kα radiation at the voltage of 45 KV and current of 40 mA. The Raman profiles were conducted over a Renishaw in Via Raman microscope with an excitation wavelength of 532 nm. The FT-IR spectra were collected by a Nicolet 6700 FT-IR spectrometer. ^{13}C-NMR spectrum was carried out using a Bruker Advance III HD 500 spectrometer. X-ray photoelectron spectroscopy (XPS) was measured on a Thermo ESCALAB 250 instrument with Al Kα radiation. Elemental analysis (EA) was carried out on a Vario EL instrument.

CO_2 temperature-programmed desorption (CO_2/O_2-TPD) were performed on the AutoChem 2920 instrument. Firstly, ca. 100 mg of a catalyst was preheated at 180 °C for 1 h under pure He. After cooling to 50 °C, the catalyst was exposed to 5%CO_2/He (20 mL/min) for 1 h. The catalyst was then purged with pure He for 1h (20 mL/min). Finally, the CO_2-TPD curves were obtained from 50 to 350 °C at a heating rate of 10 °C/min.

In situ characterization

Quasi-in situ diffuse reflection infrared Fourier transform spectroscopy (*Quasi-in situ* DRIFTS): *Quasi-in situ* DRIFTS were recorded using an ALPHA II spectrometer in the range of 4000-650 cm^{-1} with 16 scans at a spectral resolution of 2 cm^{-1}. Firstly, the benzonitrile (10 mL) and catalyst (40 mg) were carefully added into a 100 mL three-necked flask. Then, the reaction system was purged with 5wt.% H_2S for three times. A gas mixture containing 5wt.% H_2S and balance N_2 was fed into the reactor under a flow rate of 20 mL/min at 60 °C for 30 min. Afterward, continuous sampling is conducted every two minutes and quickly transferred to the ALPHA II spectrometer for testing. Finally, DRIFTS spectra were collected. *Quasi-in situ* Raman spectra were collected by a Renishaw spectrometer laser beam ($\lambda = 532$ nm). Accordingly, the reaction studies were carried out at 60 °C for 16 min.

DFT calculations

We have employed the Vienna Ab Initio Package (VASP)[1-2] to perform all the density functional theory (DFT) calculations within the generalized gradient approximation (GGA) using the PBE[3] formulation. We have chosen the projected augmented wave (PAW) potentials[4-5] to describe the ionic cores and take valence electrons into account using a plane wave basis set with a kinetic energy cutoff of 520 eV. Partial occupancies of the Kohn−Sham orbitals were allowed using the Gaussian smearing method and a width of 0.05 eV. The electronic energy was considered self-consistent when the energy change was smaller than 10^{-5} eV. A geometry optimization was considered convergent when the force change was smaller than 0.02 eV/Å. Grimme's DFT-D3 methodology[6-7] was used to describe the dispersion interactions. The free energy of a gas phase molecule or an adsorbate on the surface was calculated by the equation $G = E + ZPE - TS$, where E is the total energy, ZPE is the zero-point energy, T is the temperature in kelvin (298.15 K is set here), and S is the entropy.

Catalyst measurement

Typical procedure for the synthesis of thiobenzamide

Firstly, substrate (benzonitrile and its derivatives, 4 mmol), solvent (DMAC, 40 mL), isopropylamine (1 mL) and catalyst (40 mg) were carefully added into a 100 mL three-necked flask.

Then, the reaction system was purged with 5wt.% H_2S for three times. A gas mixture containing 5wt.% H_2S and balance N_2 was fed into the reactor at a flow rate of 20 mL/min. Subsequently, the reactor was conducted at 30-100 °C with a constant stirring speed of 800 rpm and maintained for 0.5-2 h. After the reaction, the liquid phase of the reaction mixture was analyzed by gas chromatography with a flame ionization detector (Shimadzu, GC-2010Plus). The conversion (*Con.*) and selectivity (*Sel.*) are defined as follows:

$$Con. = \frac{moles\ of\ substrate\ after\ reaction}{Initial\ moles\ of\ substrate} \times 100\%$$

$$\mathrm{Sel.} = \frac{moles\ of\ thiobenzamide}{moles\ of\ substrate\ reacted} \times 100\%$$

For the reusability evaluations, the catalysts were separated by centrifugation after the end of the reaction, and washed with ethanol for three times, followed by drying in vacuo before the next catalytic cycle.

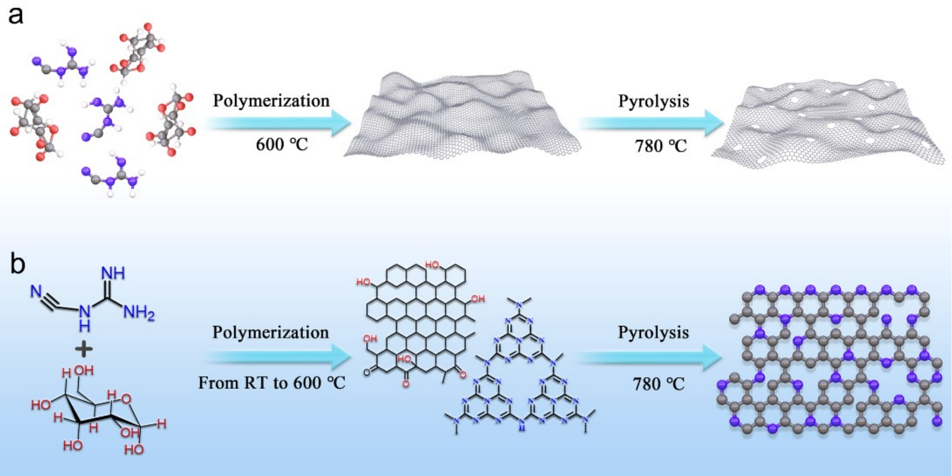

Fig. S1 (a) Schematic showing the preparation of N-GC-$_X$ catalysts, and (b) their reaction mechanism for the formation of C-N polymeric complex.

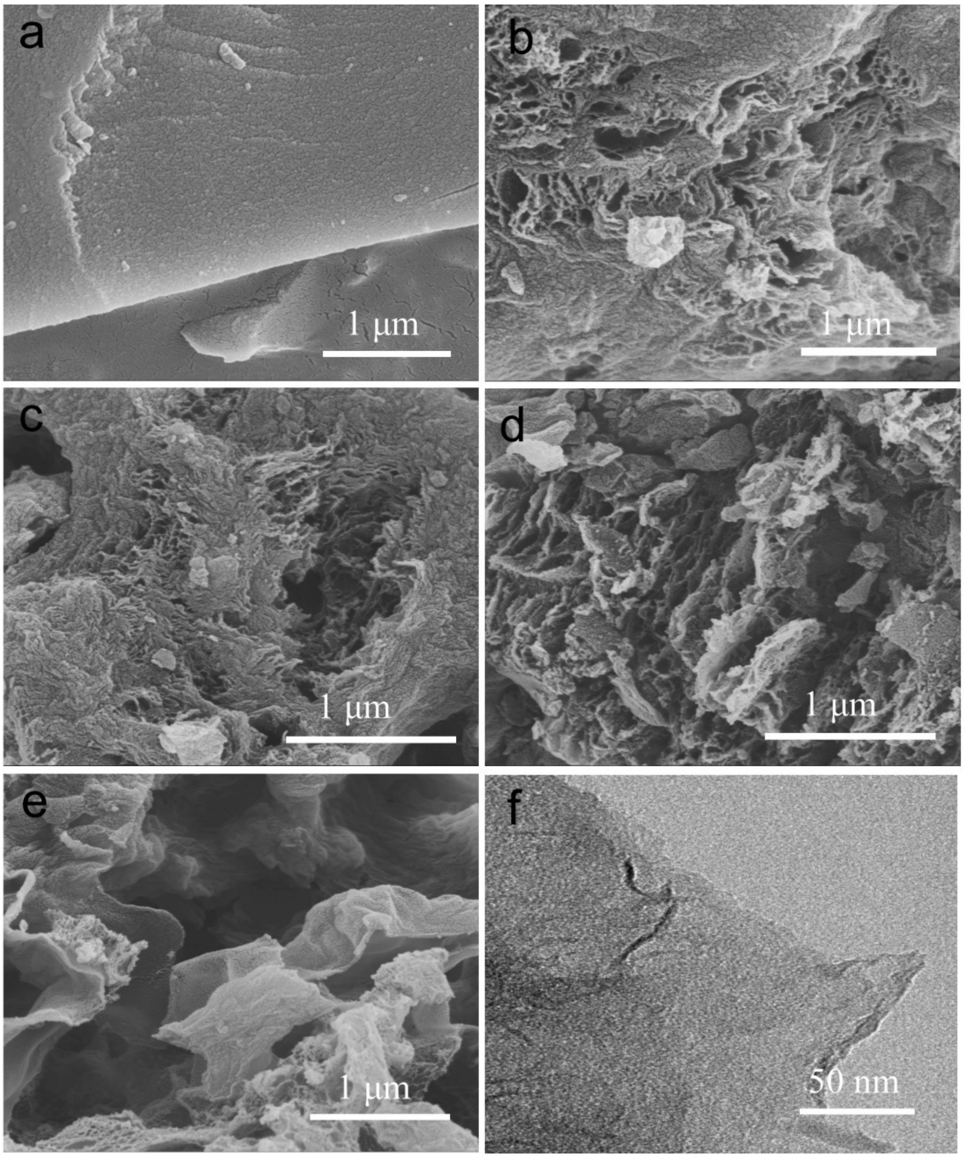

Fig. S2 SEM images of (a) pristine GC, (b) N-GC-2, (c) N-GC-4, (d) N-GC-6 and (e) N-GC-8; (f) TEM image of N-GC-6.

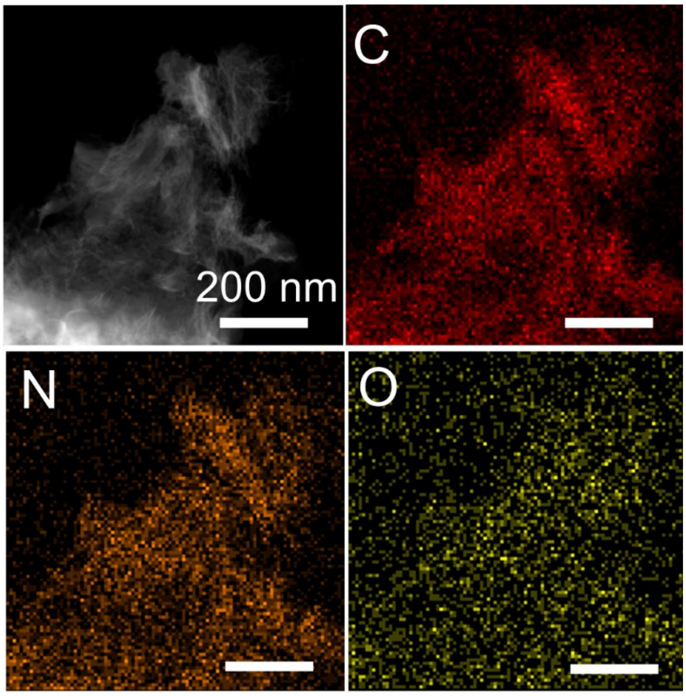

Fig. S3 STEM-EDS mappings of N-GC-6.

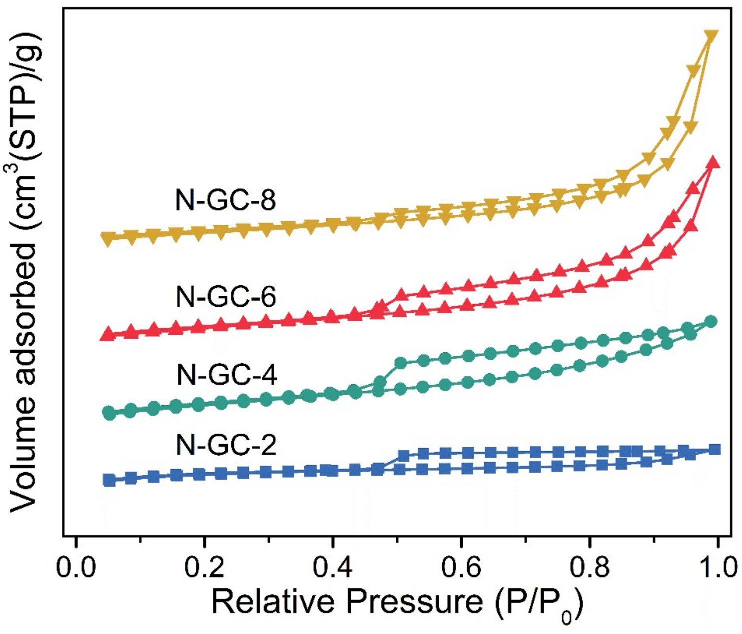

Fig. S4 N_2 sorption isotherms of N-GC-2, N-GC-4, N-GC-6 and N-GC-8.

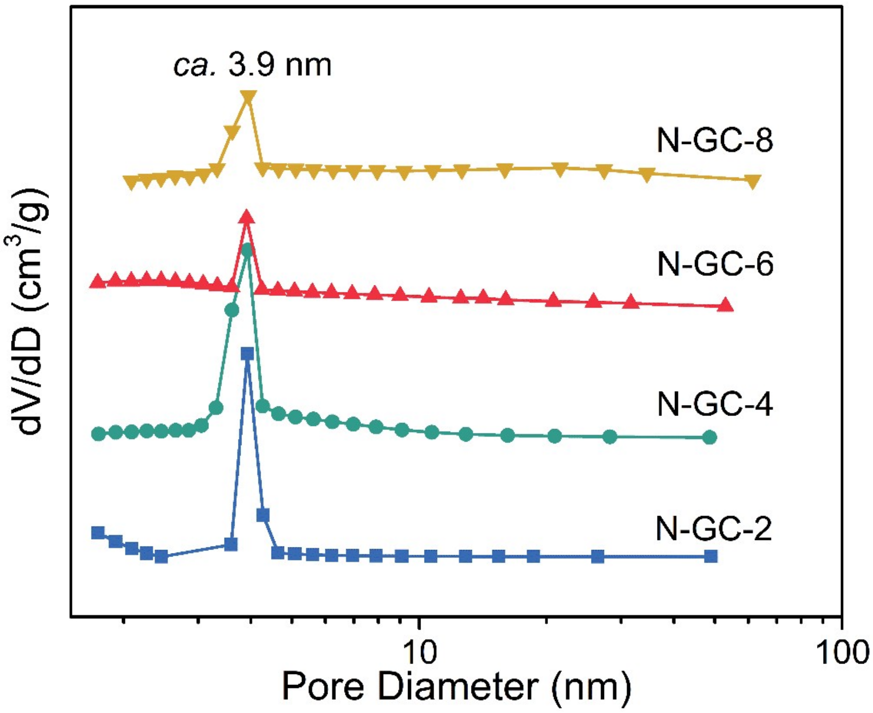

Fig. S5 Pore-size distribution of N-GC-2, N-GC-4, N-GC-6 and N-GC-8.

Table S1. Elemental composition and physical properties of pristine GC and N-GC-$_X$.

Sample	N (wt%)[a]	C (wt%)[a]	O (wt%)[a]	S_{BET} (m^2/g)[b]	Pore volume (cm^3/g)[c]
GC	4.24	84.52	8.79		
N-GC-2	21.31	59.76	16.68	408.8	0.113
N-GC-4	27.90	56.33	13.52	338.1	0.337
N-GC-6	32.1	54.57	10.15	271.8	0.555
N-GC-8	32.42	55.22	9.54	262.3	0.579

[a]Determined by elemental analysis; [b, c]Calculated from N_2-sorption isotherms.

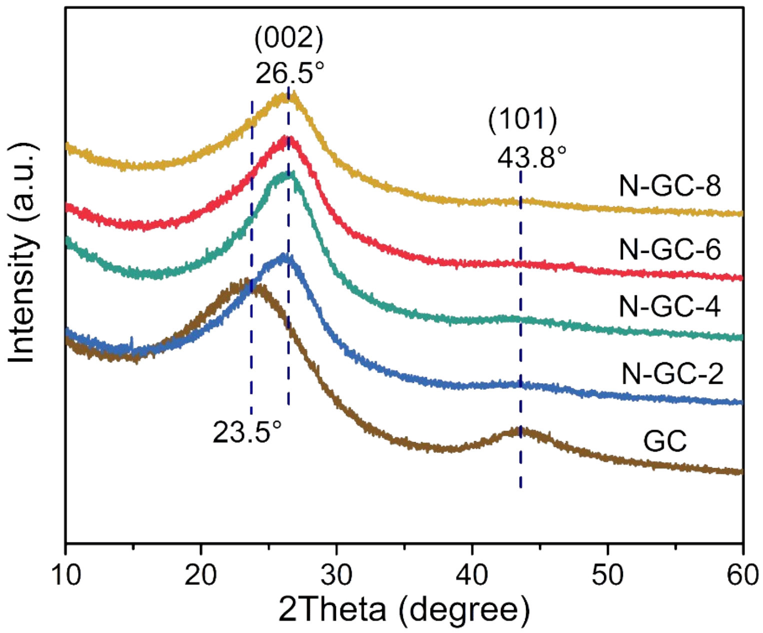

Fig. S6 XRD patterns of pristine GC and N-GC-$_X$ catalysts.

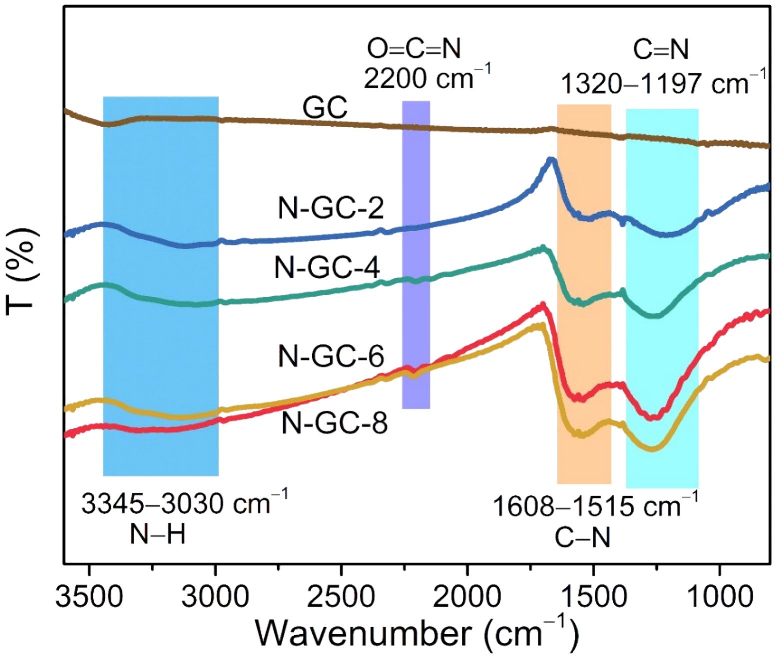

Fig. S7 FT-IR patterns of pristine GC and N-GC-$_X$ catalysts.

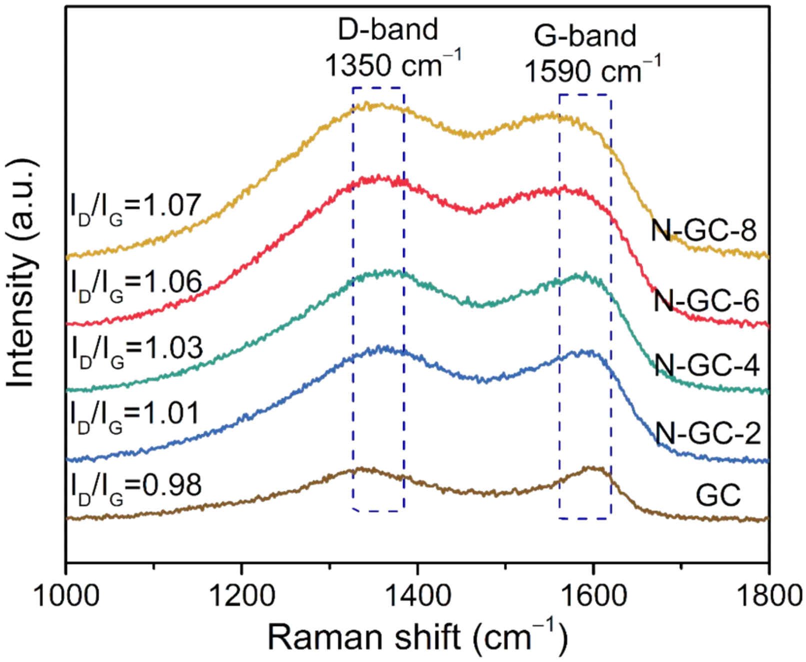

Fig. S8 Raman profiles of pristine GC and N-GC-$_X$ catalysts.

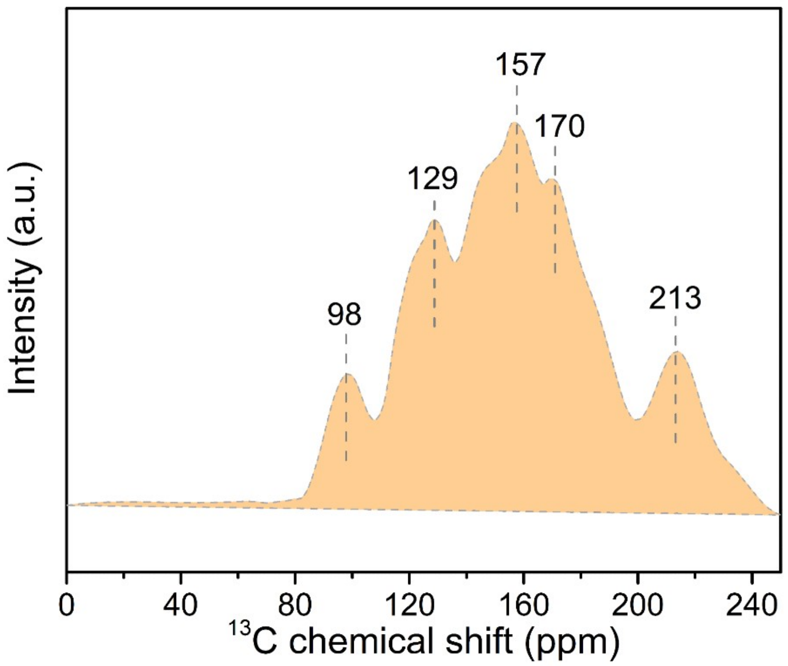

Fig. S9 ^{13}C NMR spectrum of N-GC-6.

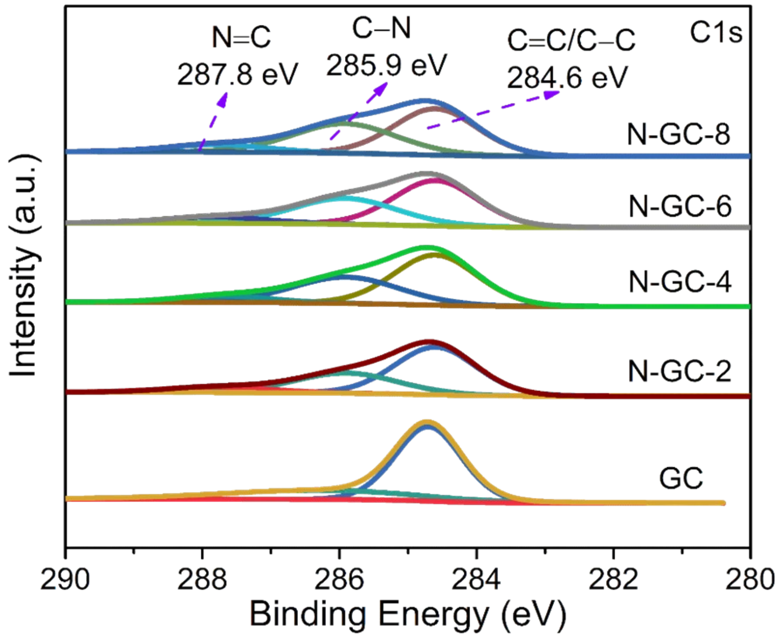

Fig. S10 C1s XPS of pristine GC and N-GC-$_X$ catalysts.

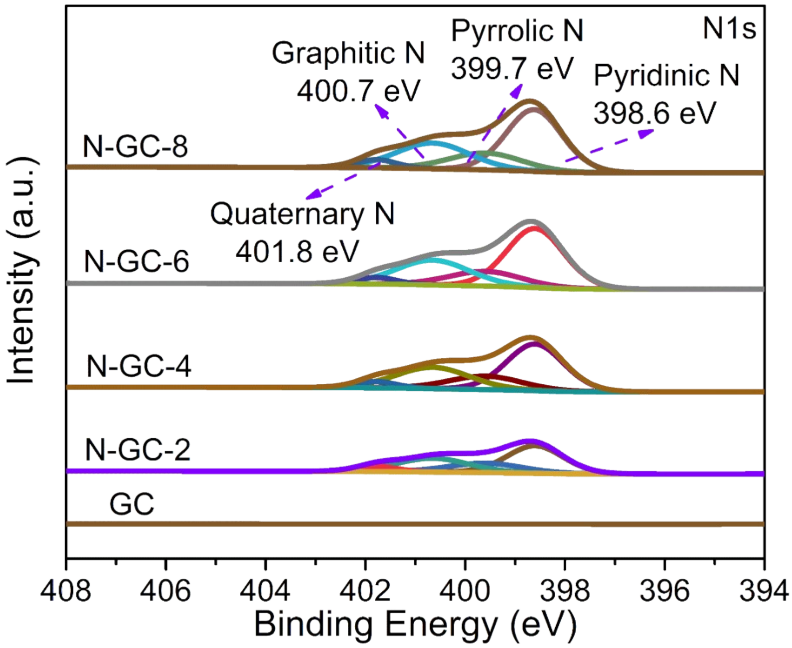

Fig. S11 N1s XPS of pristine GC and N-GC-$_X$ catalysts.

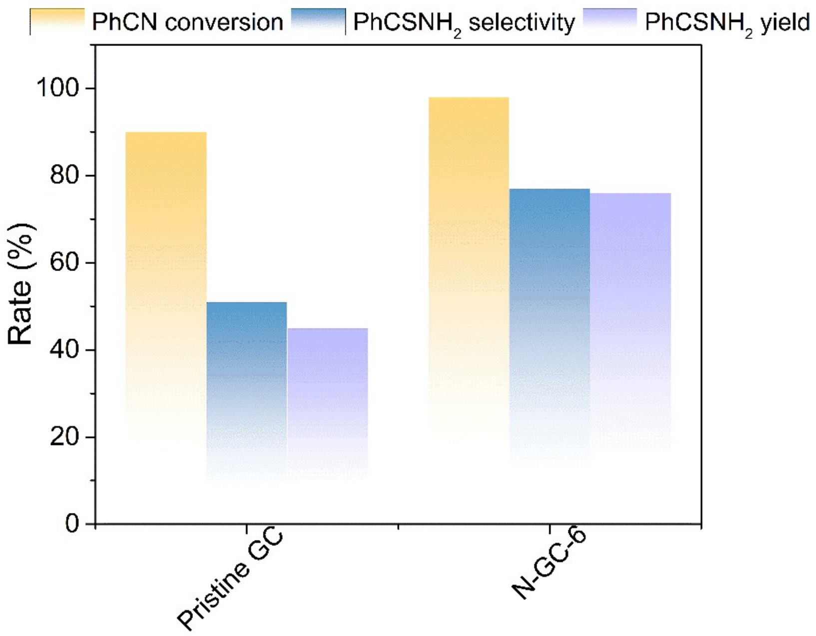

Fig. S12 Catalytic conversion of benzonitrile to thiobenzamide in the presence of pristine GC and N-GC-6.

Table S2. Optimization study of the formation of thiobenzamide.

Solvent	Temperature (°C)	Time (h)	PhCN conversion (%)	$PhCSNH_2$ selectivity (%)
DMAC	40	2	91	65
DMAC	50	2	97	72
DMAC	60	2	98	77
DMAC	70	2	98	69
DMF	60	2	93	70
DMSO	60	2	96	43
EtOH	60	2	20	43
MeOH	60	2	18	17
H_2O	60	2	100	3
DMAC	60	1	98	59
DMAC	60	3	98	80
DMAC	60	4	98	84

Reaction conditions: Benzonitrile (4 mmol), H_2S (5 wt.%, N_2 balance), Solvent (39 mL), Isopropylamine (1 mL), Catalyst (40 mg).

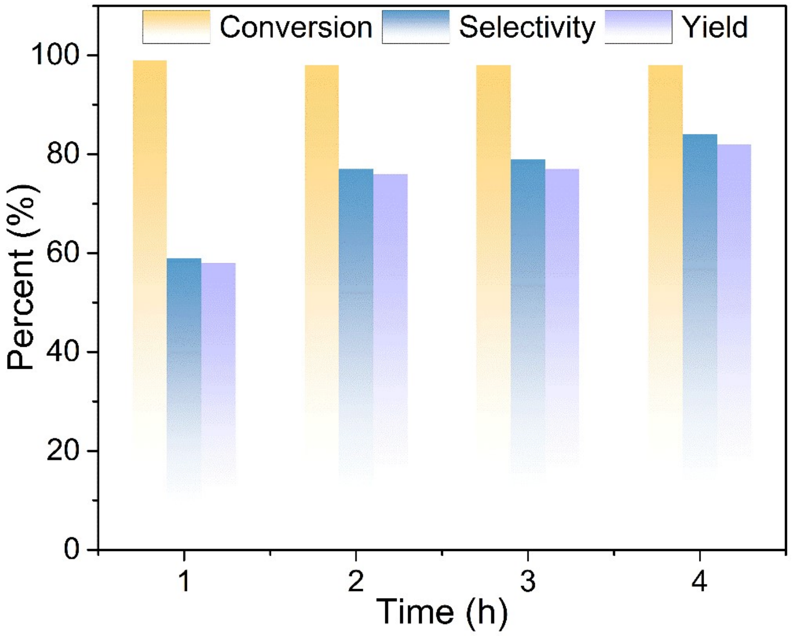

Fig. S13 Effect of reaction time on the nucleophilic addition of benzonitrile with H_2S over N-GC-6.

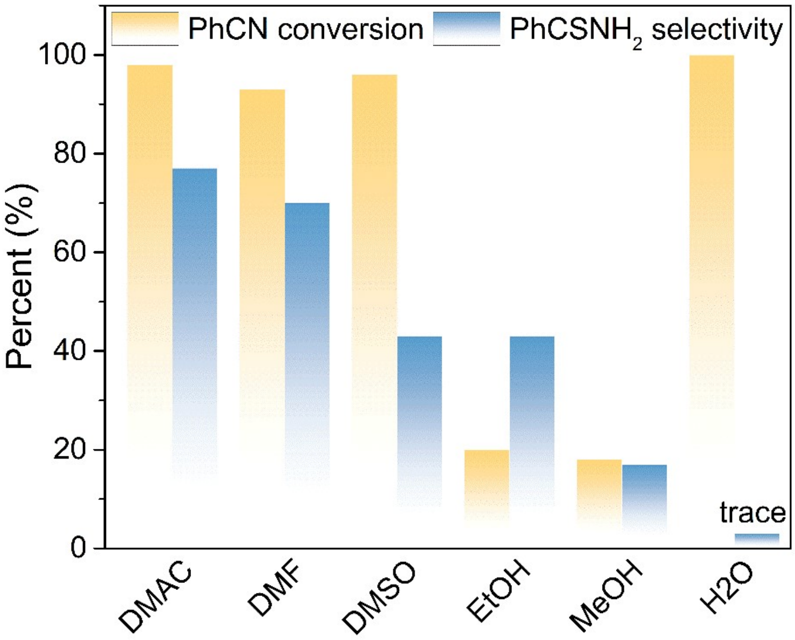

Fig. S14 Effect of reaction solvent on the nucleophilic addition of benzonitrile with H_2S over N-GC-6.

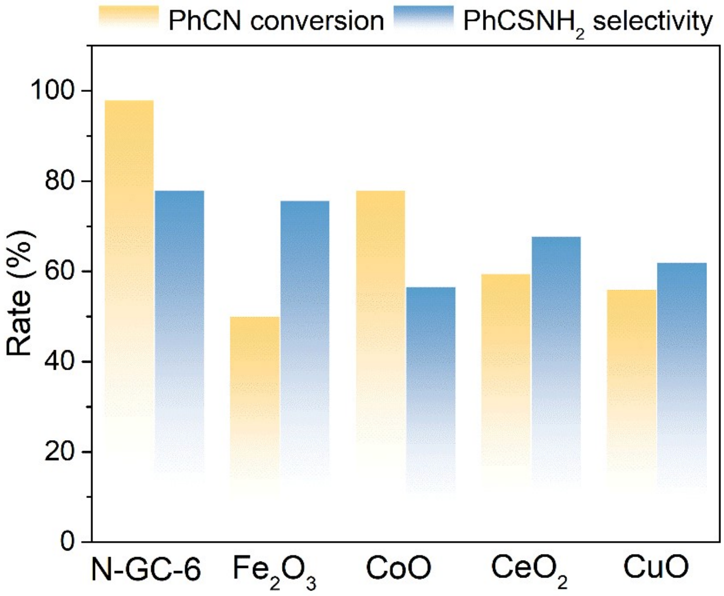

Fig. S15 Catalytic performances of H_2S nucleophilic addition of PhCN to $PhCSNH_2$ on N-GC-6, Fe_2O_3, CoO, CeO_2 and CuO.

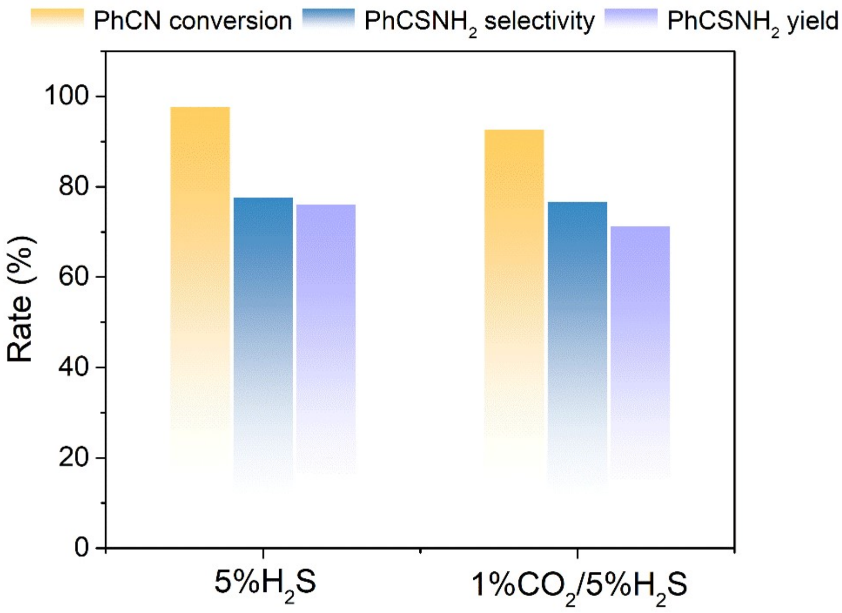

Fig. S16 Effect of CO_2 on catalytic activity over N-GC-6.

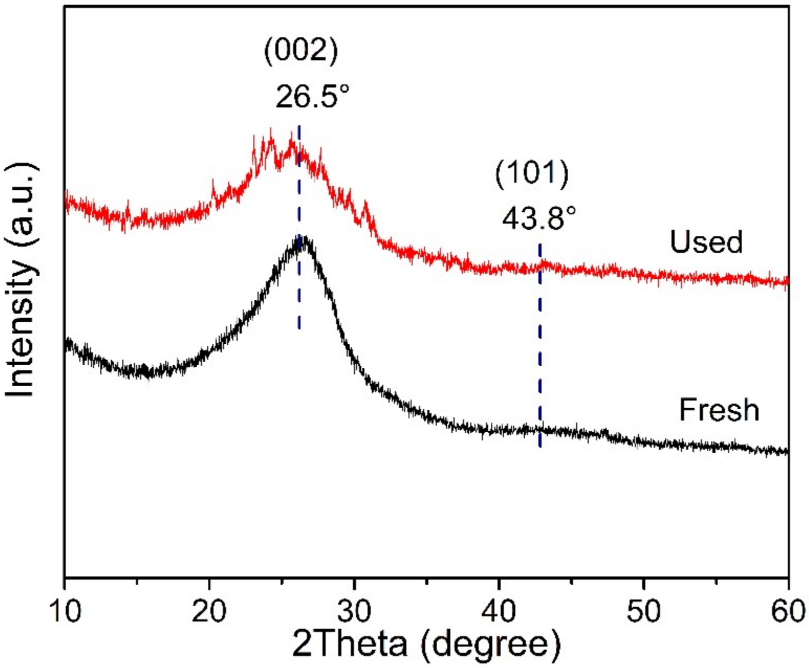

Fig. S17 XRD patterns of fresh and used N-GC-6.

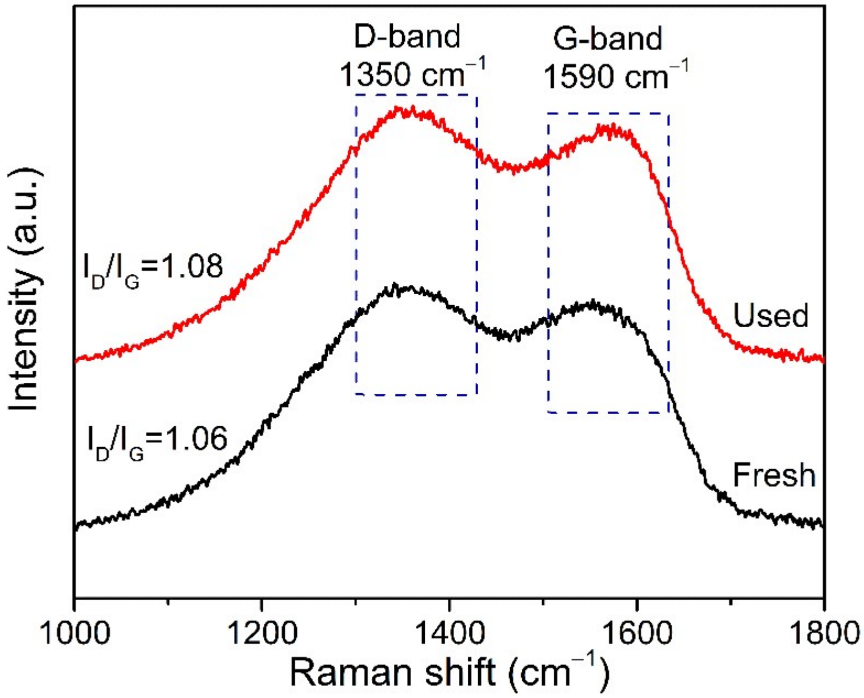

Fig. S18 Raman profiles of fresh and used N-GC-6.

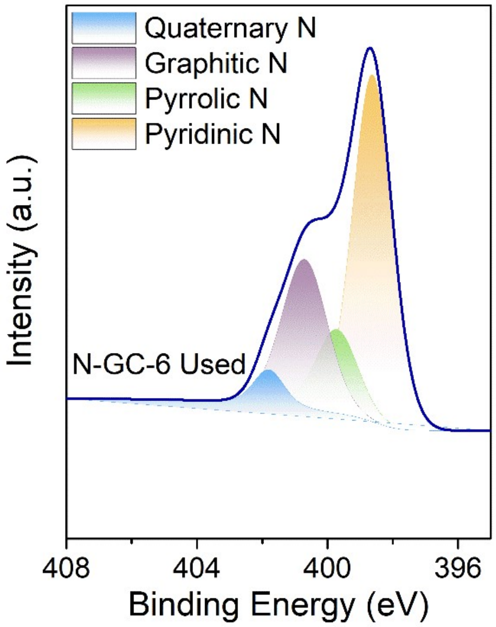

Fig. S19 High-resolution N1s XPS profiles of Used N-GC-6.

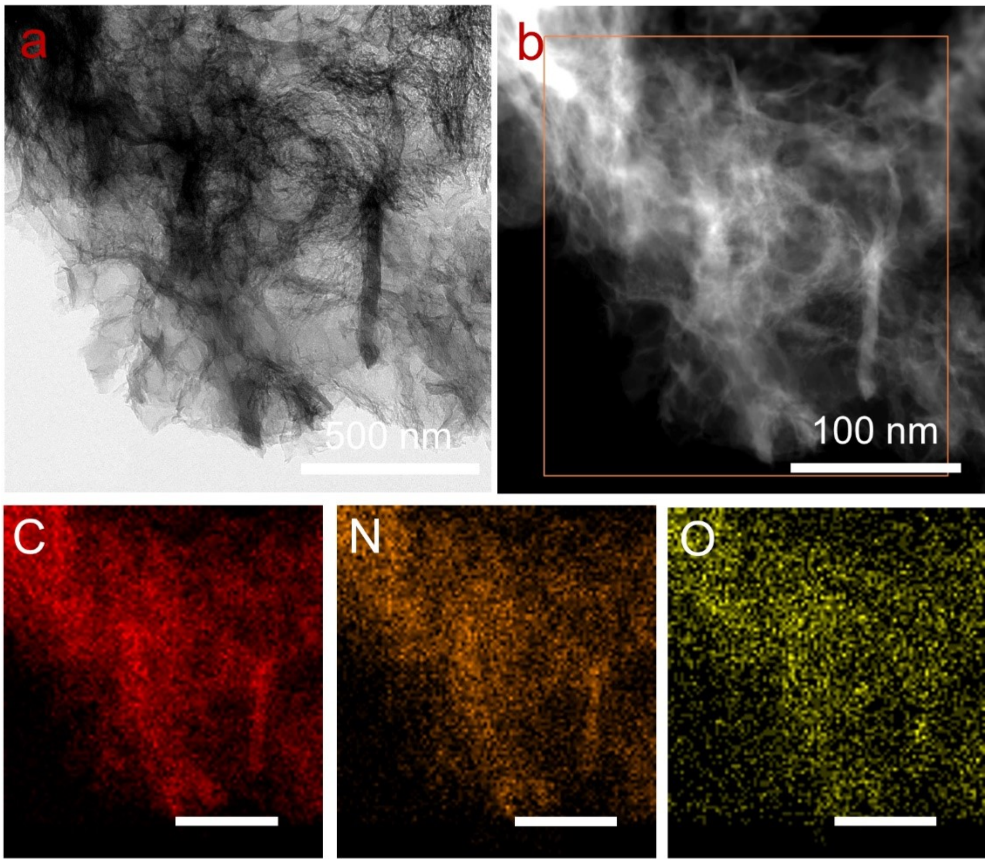

Fig. S20 (a) TEM image of used N-GC-6; (b) STEM image of used N-GC-6 and the resultant C, N and O element maps.

The outcomes of XRD (**Fig. S17**) and Raman (**Fig. S18**) analyses performed over the used catalyst verified that the chemical structure of N-GC-6 is well preserved. The N1s XPS analysis of demonstrates that the nitrogen configurations of the used catalyst did not change after the long-term cycling (**Fig. 19**). Moreover, the TEM (**Fig. S20a**) and EDS mapping (**Fig. S20b**) images of the used catalyst show morphology similar to that of fresh one, and the uniform dispersion of C, N and O over the whole architecture. The results reveal that N-GC-6 can be applied as highly efficient, durable catalysts for H_2S resource utilization in industry.

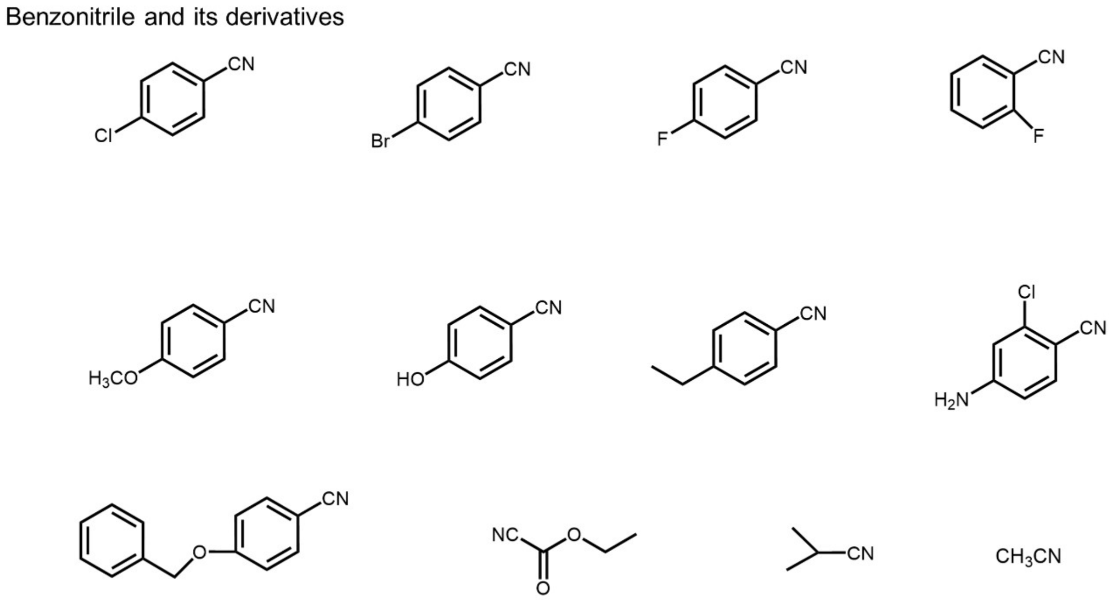

Fig. S21 Chemical structural formula of benzonitrile and its derivatives.

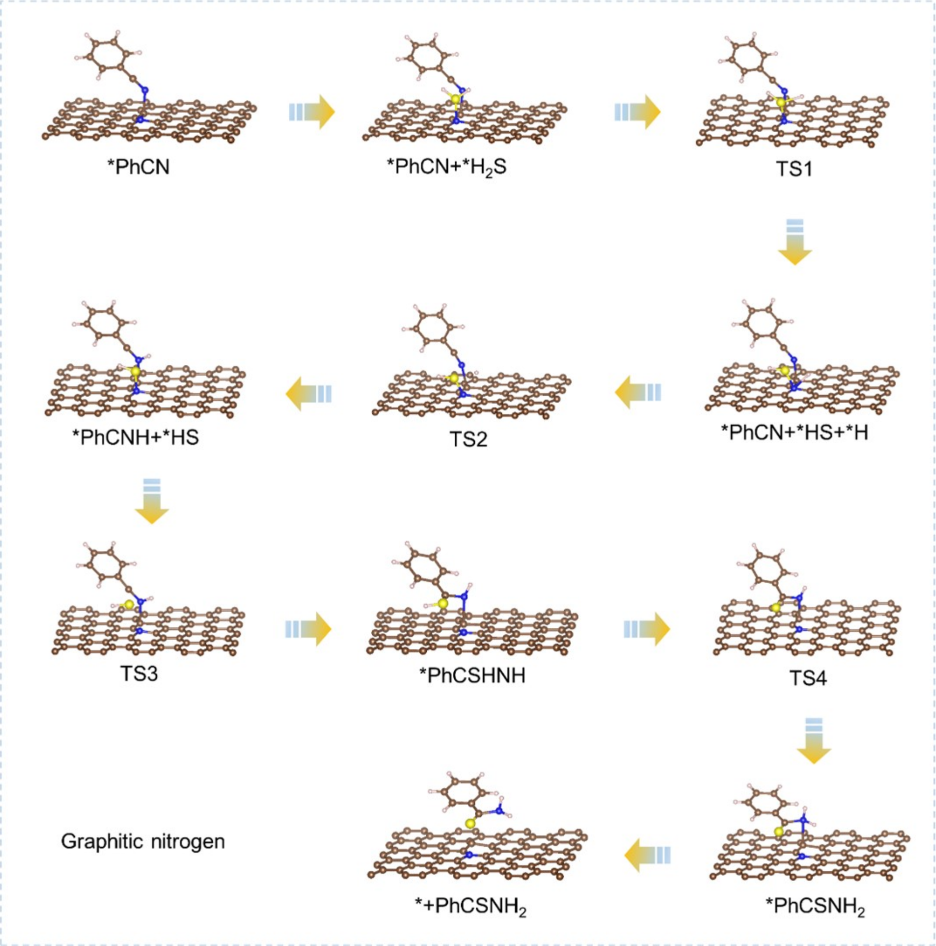

Fig. S22 The corresponding structures along the reaction paths on graphitic N.

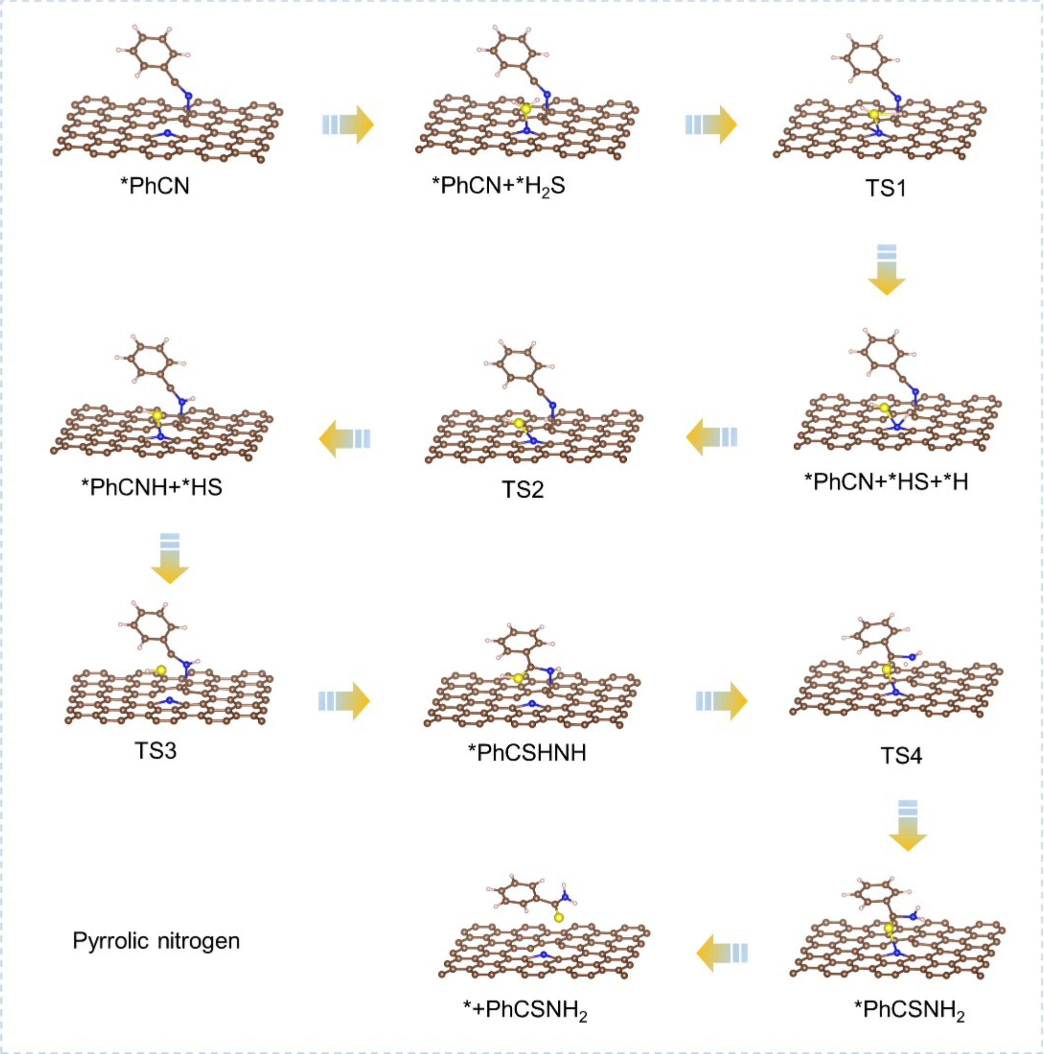

Fig. S23 The corresponding structures along the reaction paths on pyrrolic N.

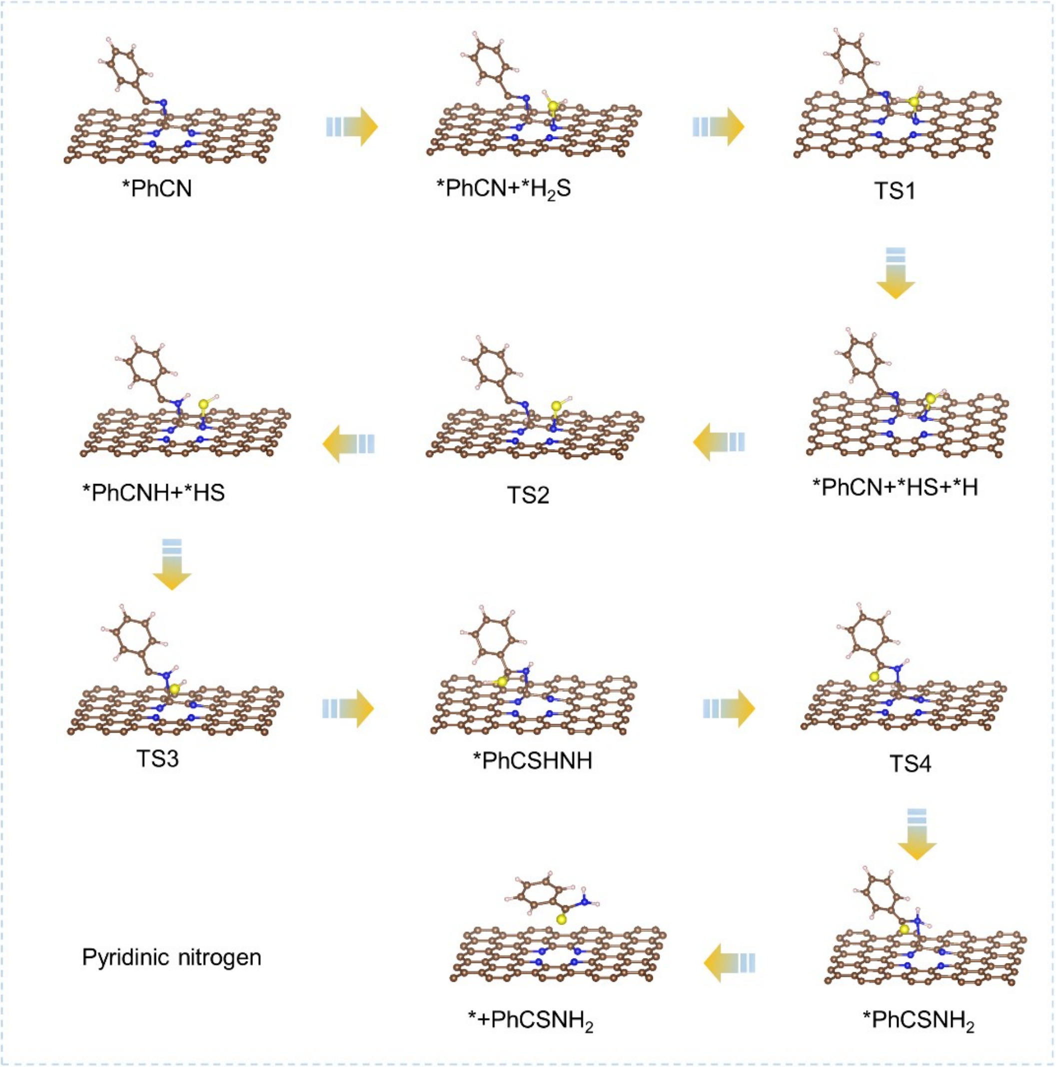

Fig. S24 The corresponding structures along the reaction paths on pyridinic N.

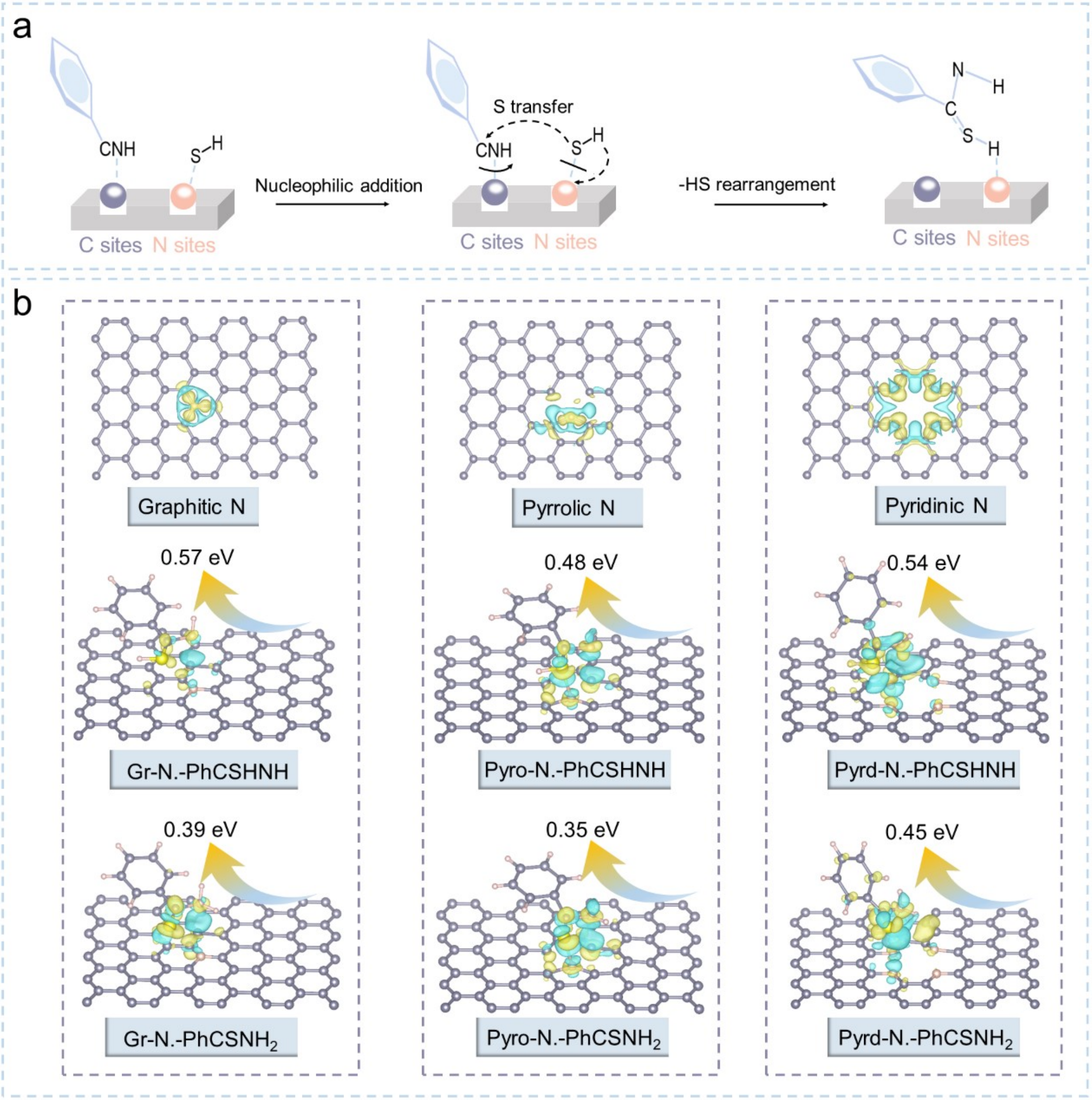

Fig. S25 (a) The proposed reaction mechanism for PhCSHNH formation mediated by nitrogen-doped carbon catalyst; (b) The charge density differences and Bader charge transfer for Ph-CSHNH and Ph-CSNH$_2$ adsorbed on graphitic N, pyrrolic N and pyridinic N.

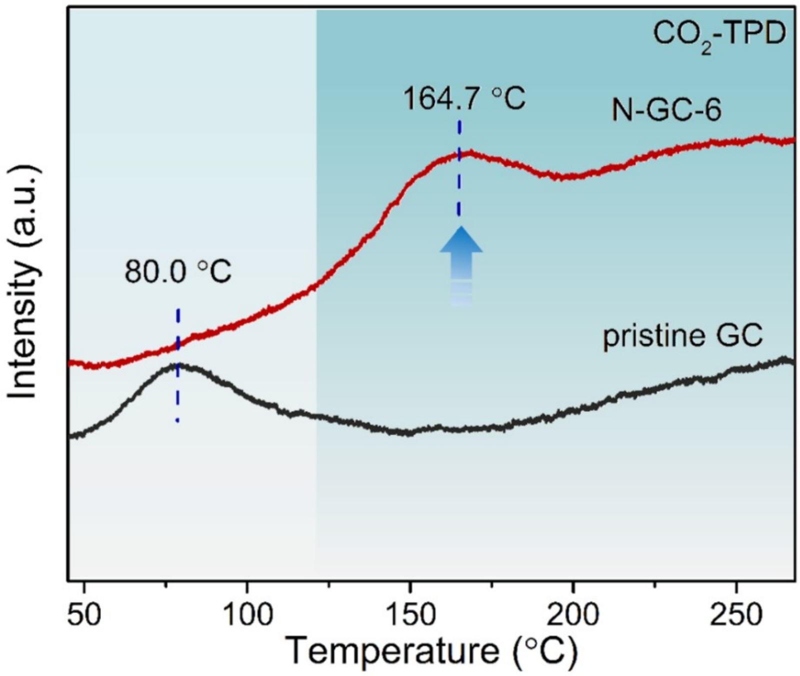

Fig. S26 CO$_2$-TPD profiles of pristine GC and N-GC-6.

CO$_2$-TPD characterizations were performed to investigate how activity is influenced by surface properties[8]. As shown in CO$_2$-TPD in **Fig. S26**, the N-GC-6 exhibits higher TPD adsorption peaks for CO$_2$ molecules when compared with pristine GC, in consistent with the DFT data that the reactants are strongly absorbed on the surface of the catalysts.

References

1. G. Kresse and J. Furthmüller, *Comput. Mater. Sci.* 1996, **6**, 15−50.
2. G. Kresse and J. Furthmüller, *Phys. Rev. B* 1996, **54**, 11169−11186.
3. J. P. Perdew, K. Burke and M. Ernzerhof, *Phys. Rev. Lett.* 1996, **77**, 3865−3868.
4. G. Kresse and D. Joubert, *Phys. Rev. B* 1999, **59**, 1758-1775.
5. P. E. Blöchl, *Phys. Rev. B* 1994, **50**, 17953−17979.
6. S. Grimme, J. Antony, S. Ehrlich and H. Krieg, *J. Chem. Phys.* 2010, **132**, 154104.
7. J. K. Nørskov, J. Rossmeisl, A. Logadottir, L. Lindqvst, J. R. Kitchin, T. Bligaard and H. Jønsson, *J. Phys. Chem. B* 2004, **108**, 17886−17892.
8. G. Li, K. He, F. Zhang, G. Jiang, Z. Zhao, Z. Zhang, J. Cheng and Z. Hao, *Appl. Catal. B* 2022, **309**, 121231.